Title
ELEVATED TEMPERATURE EROSION OF STEELS

Authors
Levy, A.
Yan, J.
Patterson, J.

Publication Date
1985

Lawrence Berkeley Laboratory
UNIVERSITY OF CALIFORNIA

Materials & Molecular Research Division

To be presented at the International Conference on Wear of Materials - 1985, Vancouver, British Columbia, April 14-18, 1985; and submitted to Wear

ELEVATED TEMPERATURE EROSION OF STEELS

A. Levy, J. Yan and J. Patterson

January 1985

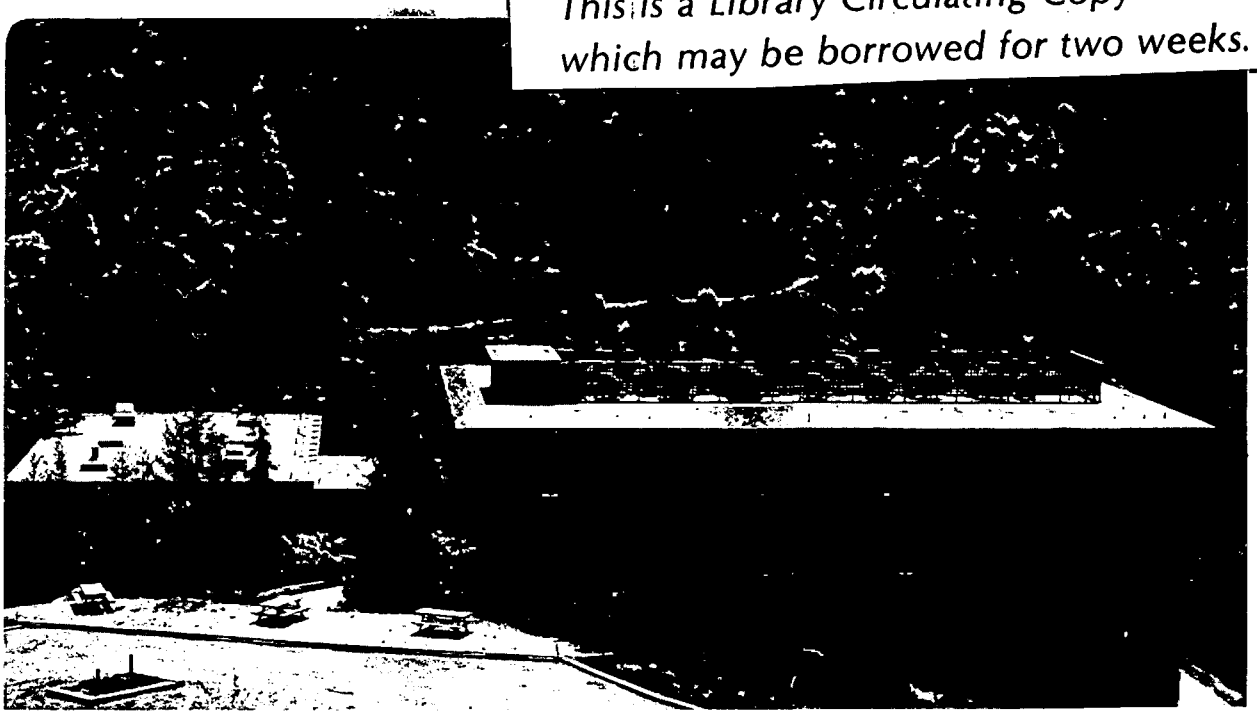

Prepared for the U.S. Department of Energy under Contract DE-AC03-76SF00098

DISCLAIMER

LBL 18256

ELEVATED TEMPERATURE EROSION OF STEELS

By

Alan V. Levy, Johnny Yan and Jennifer Patterson
Materials and Molecular Research Division
Lawrence Berkeley Laboratory
University of California
Berkeley, CA 94720
USA

Research sponsored by the U. S. Department of Energy under DOE/FEAA 15 10 10 0, Advanced Research and Technical Development, Fossil Energy Materials Program, Work Breakdown Structure Element LBL-3.5 and under Contract No. DE-AC03-76SF00098.

ABSTRACT

The elevated temperature erosion behavior of several commercial, ferritic and austenitic steels was determined over a range of temperatures from room temperature to 900°C. It was determined that all of the steels had constant or decreasing erosion rates as the test temperature was increased until a temperature was reached where a marked increase in erosion rate began to occur with temperature. Austenitic steels were determined to have lower erosion rates than ferritic steels and hardness had no correlation with erosion rate. All of the steels tested eroded by the platelet mechanism of erosion.

INTRODUCTION

The use of structural steel alloys in the erosion-corrosion environments of coal conversion and utilization plant components has resulted in many instances of unacceptable levels of surface degradation. The purpose of this investigation was to determine the erosion rates and mechanisms of several commercial steel alloys used in process plants and boilers. Low alloy and stainless steels were investigated at temperatures from room temperature to beyond their normal use temperature in near inert gas atmospheres. Heat treatable steels were tested in the range of their heat treatment temperatures to determine whether changes in erosion behavior occurred when microstructural changes were occurring in the alloys.

In order to restrict the surface behavior occurring to erosion and not have simultaneous corrosion complicate the analysis of the active erosion mechanisms, undried nitrogen was used to carry the erodent through the nozzle. Therefore the test results obtained cannot be used

directly to predict metal loss rates in plant environments. The investigation reported herein is unique in that only erosion occurred at the elevated test temperatures. Other investigations that combined erosion and corrosion[1-3] determined that under most all test conditions corrosion is the dominant mechanism and that the erosion of corrosion scale products is occurring in combined testing and not the erosion of the substrate metal.

EXPERIMENTAL CONDITIONS

The alloys tested in this investigation are listed in Table 1 along with representative compositions from the literature. They were selected to have a variety of metallurgical responses to elevated temperature exposure and to have a varying chromium content to resist the partial pressure of oxygen in the undried nitrogen. The materials were obtained from flat sheet or from 2.5 cm thick pipe sections. In the latter case, the specimens were run through rolls to produce 0.3 cm thick pieces. The materials were fully annealed prior to testing or, in the case of 410SS and 17-4PH, heat treated as indicated in Table 1. The specimens were 5 cm X 2 cm X 0.3 cm and were polished prior to testing to a 240 or 600 grit finish.

The room temperature erosion tests were conducted using the nozzle type tester described in Reference 4. The elevated temperature tests were carried out in the elevated temperature tester shown in Figure 1. The specimen and carrier gas stream temperatures were controlled within 10°C. This piece of equipment operates in the same manner as the room temperature erosion tester. A single, filament wound furnace

encapsulates the gas-particle mixing chamber, nozzle and specimen holder as well as a several foot long, coiled heat exchanger placed around the nozzle that heats the undried nitrogen carrier gas prior to its entering the mixing chamber.

The elevated temperature erosion tests were generally conducted in one cycle using 300g of 240-325μm mean dia silicon carbide particles and a 10g/min particle loading. Some of the tests on the 410SS were carried out incrementally. The specimen was preheated in the apparatus with a flow of nitrogen passing over it. The particles impinged upon the specimen surface at several velocities that were controlled by varying the pressure drop across the nozzle in a calibrated manner at impingement angles of either $\alpha=30^{\circ}$ or 90°. The pressure setting was determined by using a computer program described in Reference 5 which accounts for the elevated temperature of the gas-particle stream.

After completion of the experiment the specimen was quickly transferred to a cold nitrogen flow and cooled to below $250^{\circ}C$ to prevent oxidation. Some oxidation of the specimens did occur, especially on the low chromium content specimens at the higher temperatures. The cooled specimens were weighed on an analytical balance accurate to 10^{-4}g after being cleaned with alcohol in an ultrasonic cleaner.

RESULTS

Austenitic Stainless Steels

Types 310 and 304SS were tested at temperatures up to $900^{\circ}C$. Figure 2 plots all of the test points measured for 310SS. Four separate runs were made over the test temperature range, using a

different specimen for each test to determine the reproduceability of the tests. The locations of the data points indicates that the reproduceability is acceptable. It can be seen that there is a marked difference in the amounts of erosion and the shapes of the erosion rate v.s. temperature curves between the tests run at $\alpha=30^{o}$ and 90^{o}. At $\alpha=30^{o}$, the upper curve shows that the erosion rate remained essentially the same until a test temperature near 400°C was reached at which point a rapidly increasing erosion rate with test temperature occurred. The temperature at which the rate increase began to occur correlates with the temperature at which the short time tensile strength of 310SS begins to decrease significantly with increasing temperature, as shown in Figure 3.

The lower curve in Figure 2 that plots the erosion rate v.s. temperature at $\alpha=90^{o}$ has a minimum occurring around the same 400°C temperature at which the erosion rate began to rapidly increase at $\alpha=30^{o}$. The absolute magnitude of the erosion is near the same at both angles near room temperature but differs markedly at higher temperatures.

Figure 4 shows several micrographs of the eroded surfaces at three temperatures and two impingement angles. It can be seen from the appearance of the surfaces that the mechanism of erosion at all temperatures and both angles is the same even though the rates of erosion are different. The difference in the size of the shallow craters and platelets appears to increase somewhat with test temperature, but not with impingement angle. Both impingement angles result in eroded surfaces that look the same even though the actual

amount of erosion is less at $\alpha=90^{o}$ than at $\alpha=30^{o}$. These observations verify other work that the basic mechanism of erosion of ductile metals does not change with impingement angle.[6]

Figure 5 shows a cross section of the surface area of an eroded specimen at two different magnifications. The platelets and craters that occur on the eroding surface can be seen. In the higher magnification photo, the stem of the platelet attaching it to the base metal can be seen. The severely fractured condition of the stem indicates that the platelet will probably be removed by the next impact on it.

The effect of particle velocity on the erosion rate of 310SS is shown in Figure 6. The slope of the curve, 1.23, is considerably lower than the average slope of 2.5 that is measured in room temperature tests for alloy steels in the range of velocities used in these tests.[7] The erosion rate for the V=30 m/s test plotted in Figure 2 is lower than the rate for the V=30 m/s test in Figure 6 because of the different impingement angles used in the two tests.

Figure 7 shows the curve of steady state erosion rate v.s. test temperature for 304SS at $\alpha=30^{o}$. This steel has a lower chromium content (18%) than the 310SS (25%). The shape of both the 304SS and 310SS curves are the same, but the erosion rates were significantly different above 400°C. Where the erosion rates of both alloys began to increase rapidly with temperature, the erosion rate of the 304SS is 3 times the rate of the 310SS. Since both alloys were eroded in a low P_O, nitrogen gas atmosphere, the greater elevated temperature corrosion resistance of the 310SS should not account for the erosion rate

difference.

Table 2 lists the tensile properties of 304SS and 310SS at room and elevated temperature. It can be seen that at elevated test temperatures, the strength of the steel directly relates to its erosion resistance. The higher tensile strength of the 310SS at elevated temperatures compared to that of the 304SS results in a lower erosion rate. At room temperature, ductility relates directly to the erosion resistance of ductile metals and strength does not.[8] This difference in behavior is being studied further.

Low Alloy Steels

Three different steels with increasing chromium contents from 0 to 5% chromium were tested. The curves of erosion rate v.s. test temperature for the materials are plotted in Figure 8. It can be seen that they behave in a similar manner. Their curves slope down somewhat from room temperature to 200°C and then turn and begin to show an increasing erosion rate with test temperatures starting at around 300°C. This is the same type of pattern as was determined for the austenitic stainless steels except that for 304 and 310SS, the $\alpha=30^{\circ}$ curves do not dip prior to the temperature at which the erosion rates increase with temperature.

As the chromium content increased, the 25°C erosion rate decreased. However, cross-overs did occur, so the effect of chromium was not well defined. The general trend for all of the steels tested was to undergo an increase in erosion rate with rising test temperatures above some temperature. The decrease in erosion rates

with increasing temperature for the 1018 and 2 1/4Cr1Mo steels up to about 200°C has been observed in 310SS specimens up to 400°C. In the 310SS alloy, however, the decrease occurred only at $\alpha=90^{o}$ and not at $\alpha=30^{o}$ observed for the low alloy steels.

The eroded surfaces of the steels tested all showed that the platelet mechanism of erosion had occurred. Figure 9 shows the 1018 and 2 1/4Cr1Mo steel surfaces after erosion at the 370°C test temperature. There is an indication that oxidation is beginning to occur on the tested surface as indicated by a speckled appearance that develops even though the specimens are bathed in a nitrogen flow before, during and after each test until they have cooled sufficiently below their oxide forming temperature. Figure 10 shows the formation of oxide on the test surface for the lower chromium content steel. The 310SS specimen with 25% Cr shows no evidence of the oxidation of the test surface while the 2 1/4Cr1Mo specimen has the speckled appearance of oxidation, both having been tested near 400°C.

Another fairly common characteristic observed in the erosion of many ductile metals above the temperature where their erosion rates start to increase with test temperature is the formation of narrow, elongated gouges. These can be seen in Figure 9. They are formed by sharp, angular protrusions that occur at various angles on the erodent particles. They penetrate the soft surface of the steel and are moved along for a distance by the particles' momentum. These marks are generally not found in steels tested at room temperature.

Heat Treatment Hardenable Stainless Steels

410SS, a martensitic hardening steel, and 17-4PH, a precipitation hardening steel, were tested to determine how they respond when erosion tested in the region of their heat treatment temperatures. Also, the brittle behavior of 410SS when tempered at 475°C was studied by erosion testing at temperatures below, at, and above its temper brittle inducing temperature. The 410SS was also used to determine the precise shape of the incremental erosion rate curve when small erodent increments were used.

410SS

Incremental Erosion Rate Curve Shape

The shape of the room temperature erosion rate curves for the three different tempers of 410SS was the same and is represented by the curve for the 250°C temper material shown in Figure 11. All three materials reached steady state erosion at the same number of grams, approximately 100g. The steady state rates were 0.40 X 10^{-4}g/g for the 475°C temper, 0.43 X 10^{-4}g/g for the 250°C temper and 0.44 X 10^{-4}g/g for the 750°C temper. This indicated that the mechanical properties differences that resulted from the three tempering temperatures did not affect the erosion rate of the alloy, even the temper embrittling tempering temperature. All three materials had a flat, steady state portion of the curve as shown for the 250°C temper material in Figure 11.

The interesting part of the curve is the part prior to reaching steady state erosion. In previous work[6] the weight measurement increments were greater than the 2g of erodent increments used in this

work and only the one, highest peak was observed. In the current study, a number of peaks and valleys occur as the curve oscillated in a dampened manner to steady state erosion. The curves for all three tempers had four peaks and their complementary valleys before reaching steady state erosion. This behavior can be explained by the platelet mechanism of erosion as discussed in References 6 and 9. Figure 12 shows evidence of platelets on the cross section of the 250°C tempered 410SS.

Elevated Temperature Erosion Rates

The effect of the tempering temperature and the particular effect of the temper brittle tempering temperature had no impact on the elevated temperature erosion rate of the 410SS. Figure 13 plots the results of all three tempers on one curve of erosion rate v.s. test temperature. The curve does not show the absolute level of erosion rate for the two higher temperature tempered conditions as tests were not performed on them at 250°C. There were no breaks in the curve to account for the test being carried at a particular tempering temperature. The shape of the curve is the same one that occurred for 310SS, 1018 and 5Cr1/2Mo steels. The reduction in the rate of erosion at the intermediate temperatures was greater than occurred for the other steels.

17-4PH

The 17-4PH stainless steel in the heat treated condition behaved in the same manner as most of the other steels tested, having a minimum erosion rate at intermediate test temperatures. Figure 14 shows that testing in the range of the heat treatment temperature did not cause

any breaks to occur in the curve. The appearance of the eroded surface shown in Figure 15 at three test temperatures was typical of that which occurred for all of the alloys tested, typical shallow craters and platelets. However, no sharply defined gouges occurred.

Comparative Erosion Rates

The bar graphs in Figures 16 and 17 show how the steady state erosion rates of all of the materials tested compared at 25° and 250°C. Austenitic steels had considerably lower erosion rates than the ferritic steels. Heat treatment hardness levels had no relation to erosion rates.[9] The 410SS erosion rate dropped into the range of the austenitic steels at 250°C.

DISCUSSION

Effect of Test Temperature on Erosion Rate

All of the steels tested either had an initial decrease in their steady state erosion rate as the test temperature increased above room temperature or had a relatively flat response to test temperature. At some elevated temperature, depending upon the particular alloy, the erosion rates began to increase from the minimum value. The stainless steels had enough chromium in them to not corrode in the undried nitrogen atmosphere and, so, could be tested to higher temperatures without forming an oxide scale. Their erosion rates reached or exceeded their room temperature rates at the higher test temperatures.

It is postulated that the initial decrease in the erosion rate was due to an increase in the overall ductility of the bulk of the test specimen and a decrease in its sub-surface work hardening. While the

short time tensile elongation remained level or even decreased somewhat for some of the alloys up to 400°C the impact strength of some of he alloys increased with temperature. This distributed the force of the impacting particles by plastic deformation of the sub-surface region enough to reduce the magnitude of the localized stresses that develop in the immediate vicinity of each particle impact zone. This reduced the amount of extrusion, forging and fracture of platelets at the eroding surface and, hence, the erosion rate. It is known from room temperature testing[9, 10] that the immediate surface region undergoing erosion by small solid particles is heated to relatively high temperatures by the severe plastic deformation that occurs. Therefore, the bulk metal temperature primarily affects the sub-surface behavior of the material.

The increase in the erosion rate at higher elevated temperatures appears to start at the same temperature at which the short time, elevated temperature tensile test curve increases its downward slope. A detailed explanation to account for this beyond the overall reduction of strength of the metal at higher temperatures has not been developed yet. At this time it is speculated that the local fracture strength of individual platelets is reduced as the result of the high bulk temperature of the metal.

Surface Morphology

The mechanism of erosion at all temperatures and impingement angles used in this investigation is the platelet mechanism.[9] It appears that as the test temperature increases, the size of the shallow

craters and platelets that are formed increases. This relates to the increase in sub-surface ductility and the decreasing hardness and effectivity of the sub-surface work hardened zone or anvil to concentrate the force of the impacting particles in the surface layer.

In some of the low alloy, ferritic steels, characteristic narrow, long gouges appear on the eroded surface during elevated temperature testing, see Figure 9. They are seldom seen on austenitic steels. The gouges are caused by penetrations of sharp edges of eroding particles. This behavior may be related to the difference in the number of active slip planes between the BCC ferritic steels and the FCC austenitic steels.

Velocity Exponent

The erosion rate v.s. velocity curve in Figure 6 is typical for log-log curves for erosion. The low velocity exponent of 1.23 for this curve which represents a series of tests performed at 800°C is only one-half of the exponent values measured in room temperature testing of the same type of alloy.[7] Thus, there is a significant effect of test temperature on the distribution of the kinetic energy of the impacting particles in the target material. There does not appear to be the same correlation between erosion rate and velocity exponent at elevated temperature that is used in some room temperature erosion models.[7]

Heat Treatment and Hardness Effects

There does not appear to be any readily discernible effect of testing at the heat treatment temperatures on the erosion rates of the two heat treated alloys. One is a martensitic hardening alloy, 410SS,

and the other a precipitation hardening alloy, 17-4PH. Also, room temperature hardness does not correlate with either room temperature or elevated temperature erosion rates. The lack of correlation of erosion rates with hardness and tensile strength has been reported before.[8]

The austenitic steels eroded considerably less than the ferritic steels. The austenitic steels, 304 and 310SS were tested in the fully annealed condition while the two heat treated stainless steels, 410SS and 17-4PH were tested in a hardened condition. This has been observed before[8] and is further proof that ductility and not hardness affects the erosion rates of ductile metals.

Incremental Erosion Rate Curves

The 410SS proved to be an excellent vehicle to study the detailed shape of the incremental erosion rate curves of ductile metals, see Figure 11. For small incremental weights of erodent, measurable weight loss occurred in the 410SS specimens. The explanation for the presence of an early erosion rate peak is presented in Reference 6. The oscillation of the curves for the 410SS to the point where steady state erosion occurs is a simple extension of that explanation.

The relatively small amount of erodent that is required to achieve steady state erosion, 100g in the case of the 410SS at all three heat treatments tested, and the very flat steady state erosion curve indicates that reliable extrapolation of erosion rates to long times can be made from short time erosion tests.

CONCLUSIONS

1. Many alloy steels undergo reductions in their erosion rates at intermediate elevated temperatures.

2. Subsequent increases in erosion rates at higher elevated temperatures can be related to changes in the downward slope of the short time elevated temperature tensile strength of the alloy being tested.

3. The platelet mechanism of erosion occurred for all alloys at all test temperatures and impingement angles.

4. Austenitic steels eroded less than ferritic steels.

5. Hardness did not correlate with either room or elevated temperature erosion rates.

6. There was no discernible change in the erosion behavior of heat treated steels when they were tested at their heat treatment temperatures.

7. The particle velocity exponent of 310SS eroded at 800°C was only one-half of its room temperature value.

8. The incremental erosion rate curves for 410SS tested at room temperature had several peaks of diminishing height before steady state erosion occurred.

ACKNOWLEDGEMENT

Research sponsored by the U.S. Department of Energy under DOE/FEAA 15 10 10 0, Advanced Research and Technical Development, Fossil Energy Materials Program, Work Breakdown Structure Element LBL-3.5 and under Contract No. DE-AC03-76SF00098.

REFERENCES

1. Agarwal, S. and Howes, M.A.H., "Erosion/Corrosion of Materials in High-Temperature Environments", Proceedings of AIME Conference on High Temperature Corrosion in Energy Systems, Detroit, Michigan, September 1984.

2. Nagarajan, V. and Wright, I.G., "Influence of Oxide Scales on High Temperature Corrosion-Erosion Behavior of Alloys", Proceedings of NACE Conference on High Temperature Corrosion, NACE-6, pp. 398-405, San Diego, CA, March 1981.

3. T. Tiainen, et al, "Simulation of the Erosion and Corrosion of Materials in Fluidized Bed Combustors", Proceedings of the AIME Conference on High Temperature Corrosion in Energy Systems, Detroit, Michigan, September 1984.

4. Levy, A.V., "The Solid Particle Erosion of Steel as a Function of Microstructure", WEAR 68 No. 3, p. 269, 1981.

5. Kliest, D.M., "One-Dimensional, Two Phase Particulate Flow", (M.S. thesis) Report LBL-6967, Lawrence Berkeley Laboratory, University of California, Berkeley, CA 94720.

6. Levy, A.V., Aghazadeh, M., Hickey, G., "The Effect of Test Variables on the Platelet Mechanism of Erosion", Report No. LBL-17835, Lawrence Berkeley Laboratory, University of California, Berkeley, CA 94720.

7. Finnie, I. and McFadden, D.H., On the Velocity Dependence of the Erosion of Ductile Metals by Solid Particles at Low Angles of Incidence", WEAR 48 No. 1, p. 181, May 1978.

8. Foley, T. and Levy, A.V., "The erosion of Heat Treated Steels", WEAR 91 No. 1, p. 45, October 1983.

9. Levy, A.V., "The Erosion of Metal Alloys and Their Scales", Proceedings of NACE Conference on Corrosion-Erosion-Wear of Materials in Emerging Fossil Energy Systems, P. 298, Berkeley, CA, January, 1982.

10. Emiliani, M. and Brown, R., "Erosion of Ti-6Al-4V by Spherical Silica Particles of 90° Impact Angle", Proceedings of 6th ELSI Conference, Cambridge, University, England, September 1983.

TABLE 1

Alloy	REP. COMPOSITION IN WT%							Heat Treatment
	Cr	Ni	Mo	Mn	Si	C	Fe	
1018	-	-	-	0.8	-	0.18	Bal.	Annealed at 850-900°C for 1 hour
2 1/4Cr1Mo	2.25	-	1.0	0.5	0.5 max	0.15	Bal.	Annealed at 900°C
5Cr1/2Mo	5	-	0.5	0.5	0.5 max	0.15	Bal.	Annealed at 900°C
410SS	12.5	-	-	1.0 max	1.0 max	0.15 max	Bal.	Solution treated at 925°C for 30 min. Tempered at 250°C, 425°C, 750°C
304SS	19	9	-	2.0	1.0	0.08	Bal.	Annealed at 1020°C
310SS	25	20.5	-	2.0	1.5	0.25	Bal.	Annealed at 1100°C
17-4PH	16.5	4.0	Cu 4	1.0 max	1.0 max	0.07 max	Bal.	Condition B. Hardened at 500°C

TABLE 2

STRENGTH OF 304 AND 310 STAINLESS STEELS AT ELEVATED TEMPERATURES °C

Type Steel	Hardness	Elong. % in	25° UTS KSI	400° UTS KSI	500° UTS KSI	600° UTS KSI	700° UTS KSI	800° UTS KSI	900° UTS KSI
304SS	R_B 80	55%	85	62	58	50	37	25	15
310SS	R_B 85	45%	90	80	74	65	46	30	20

FIGURES

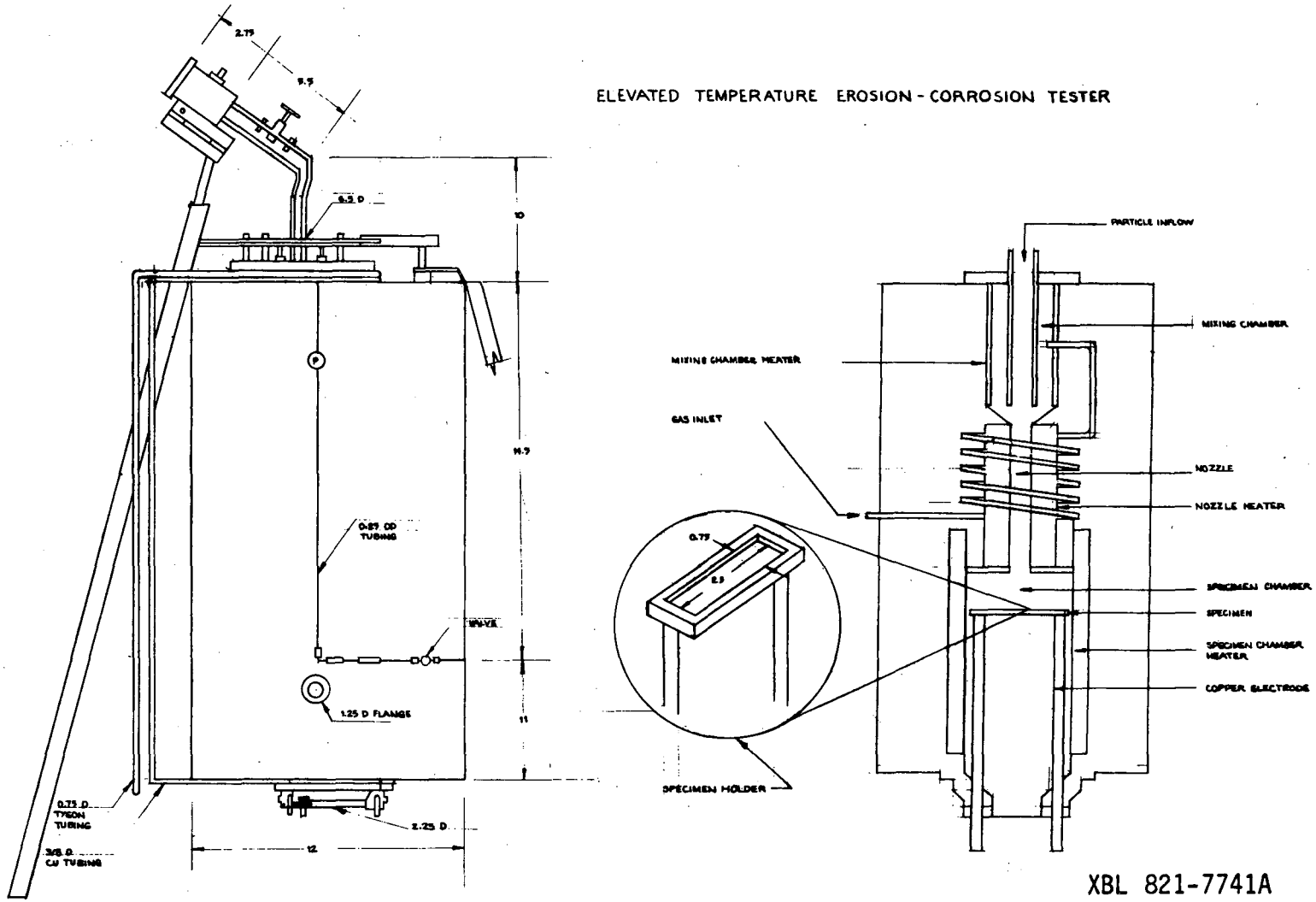

1. Sketch of elevated temperature test machine.

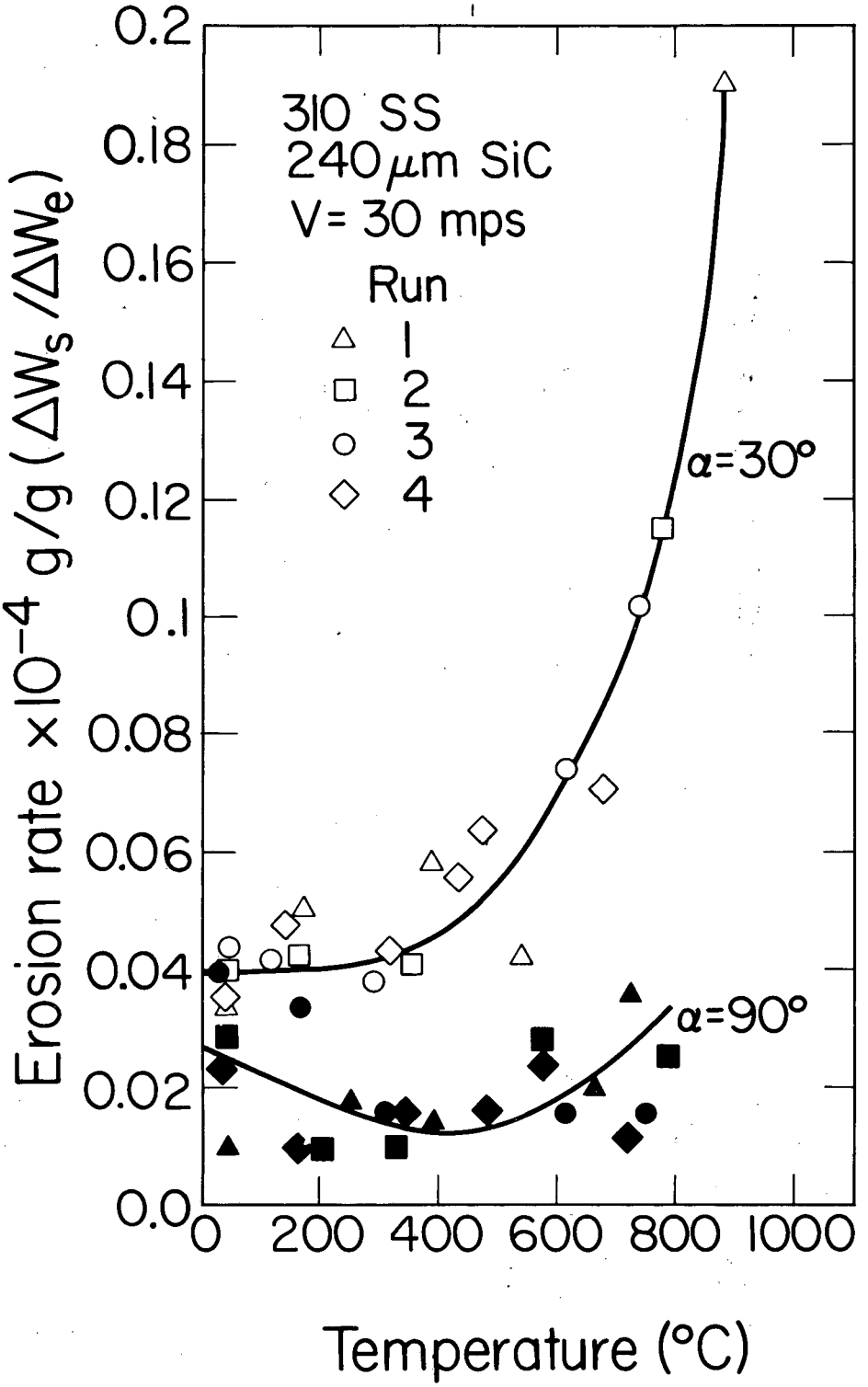

2. Erosion rate v.s. temperature for 310SS.

XBL 827-7092

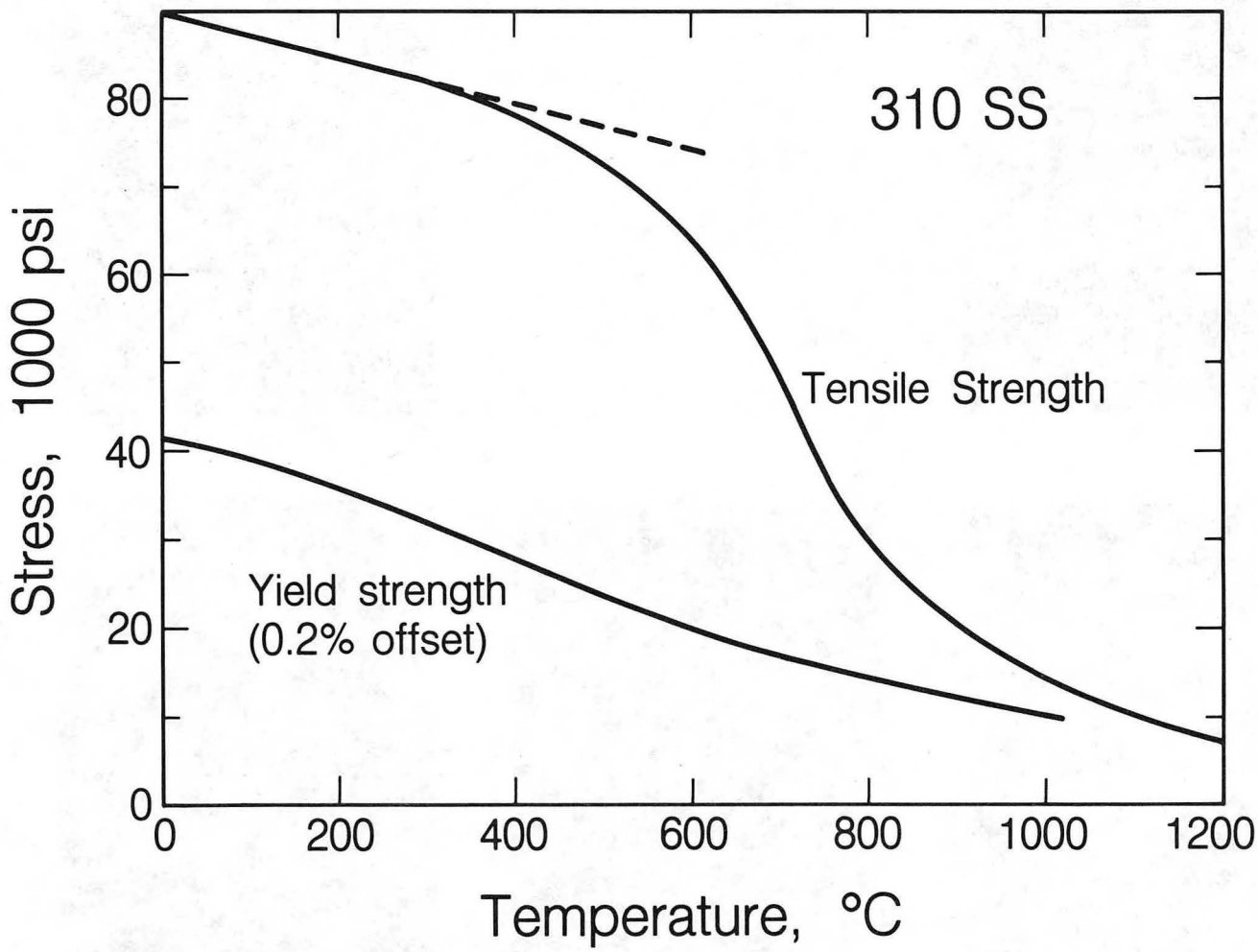

3. Short time tensile strength v.s. temperature for 310SS.

XBL 848-9892

From the "Mechanical and Physical properties of the Austenitic Chromium-Nickel Stainless Steels at Elevated Temperatures". The International Nickel Company, Inc.

30° IMPINGEMENT ANGLE

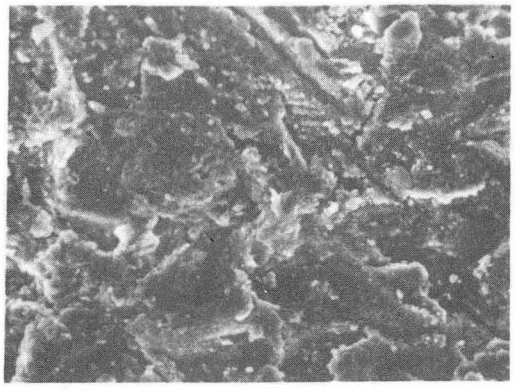

775°C

90° IMPINGEMENT ANGLE

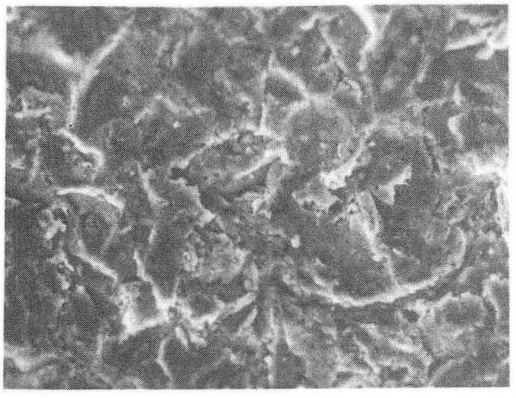

710°C

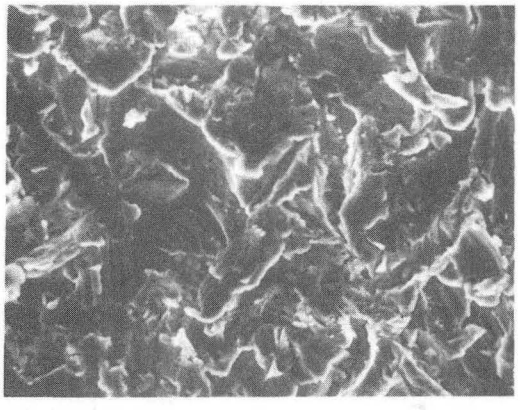

397°C

310 STAINLESS STEEL

10μm

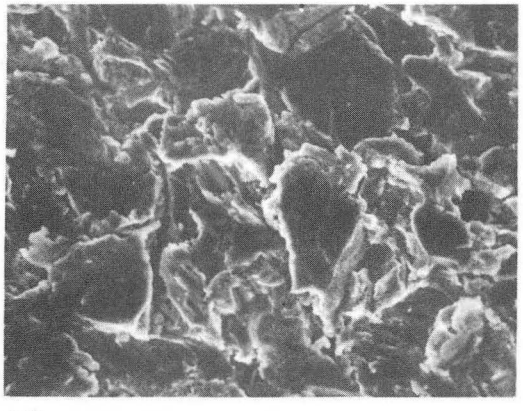

25°C

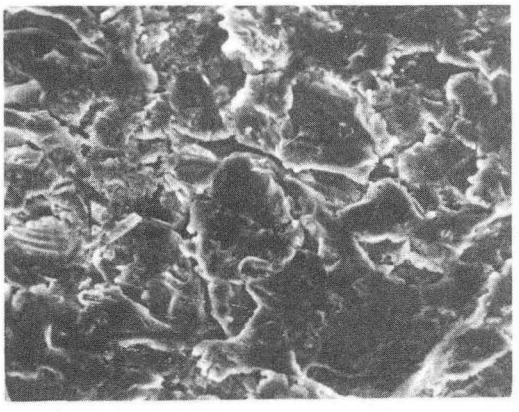

25°C

4. Micrographs of eroded 310SS surface at several test temperatures

XBB 824-3329

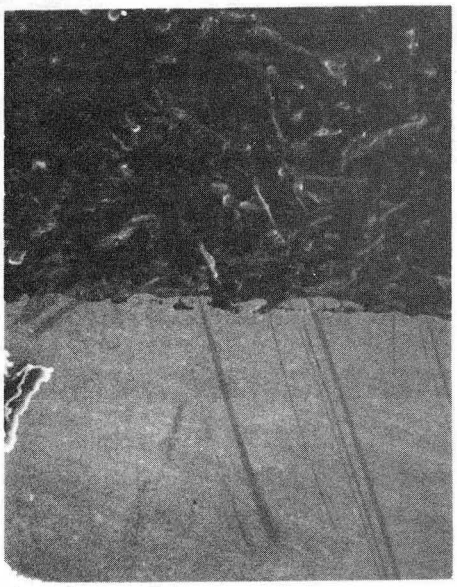

310 STAINLESS STEEL
30° IMPINGEMENT ANGLE
710°C
CROSS SECTIONAL VIEW

XBB 824-3330

5. Cross section of eroded surface of 310SS.

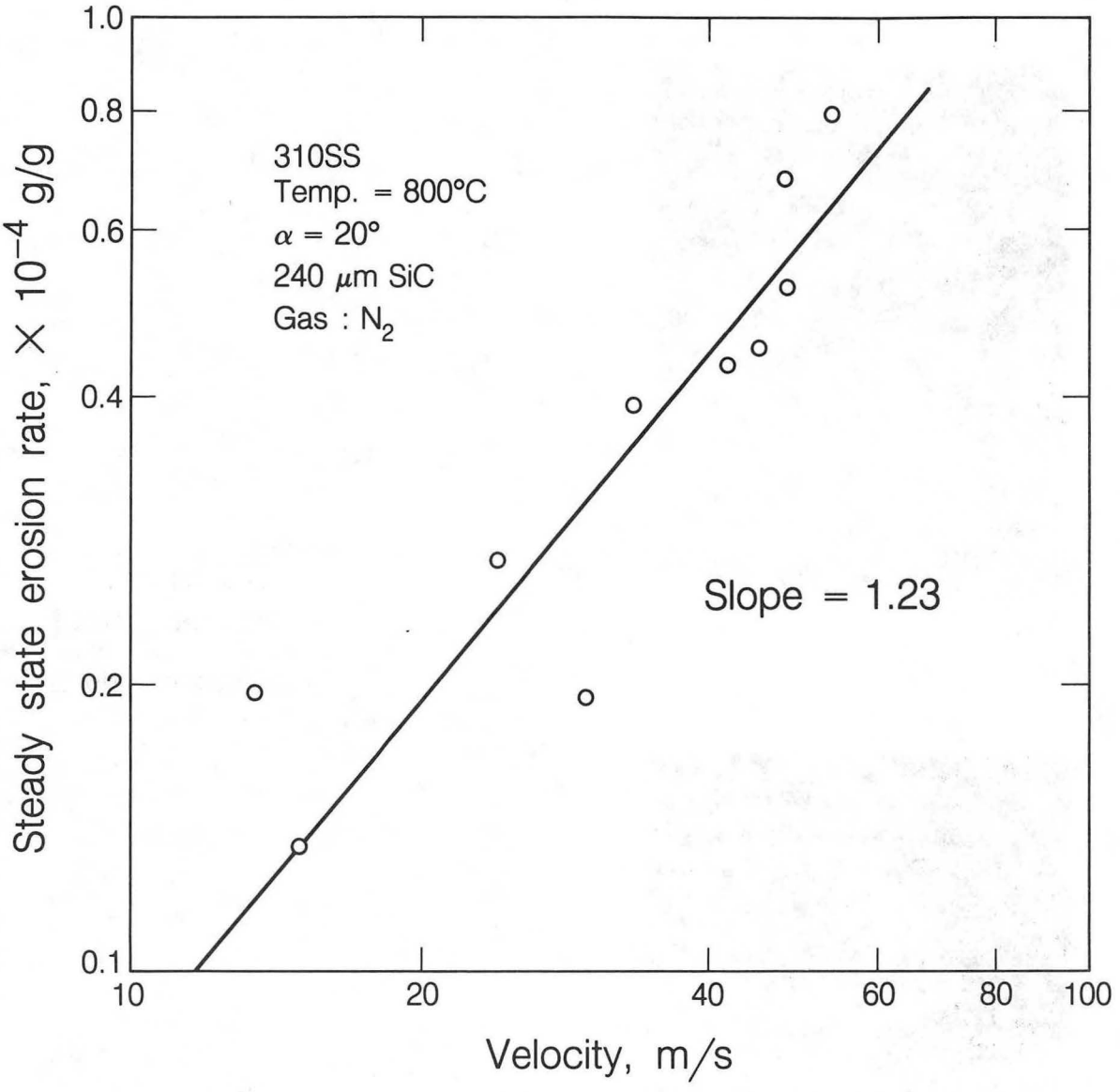

6. Erosion rate v.s. velocity for 310SS.

XBL 848-9887

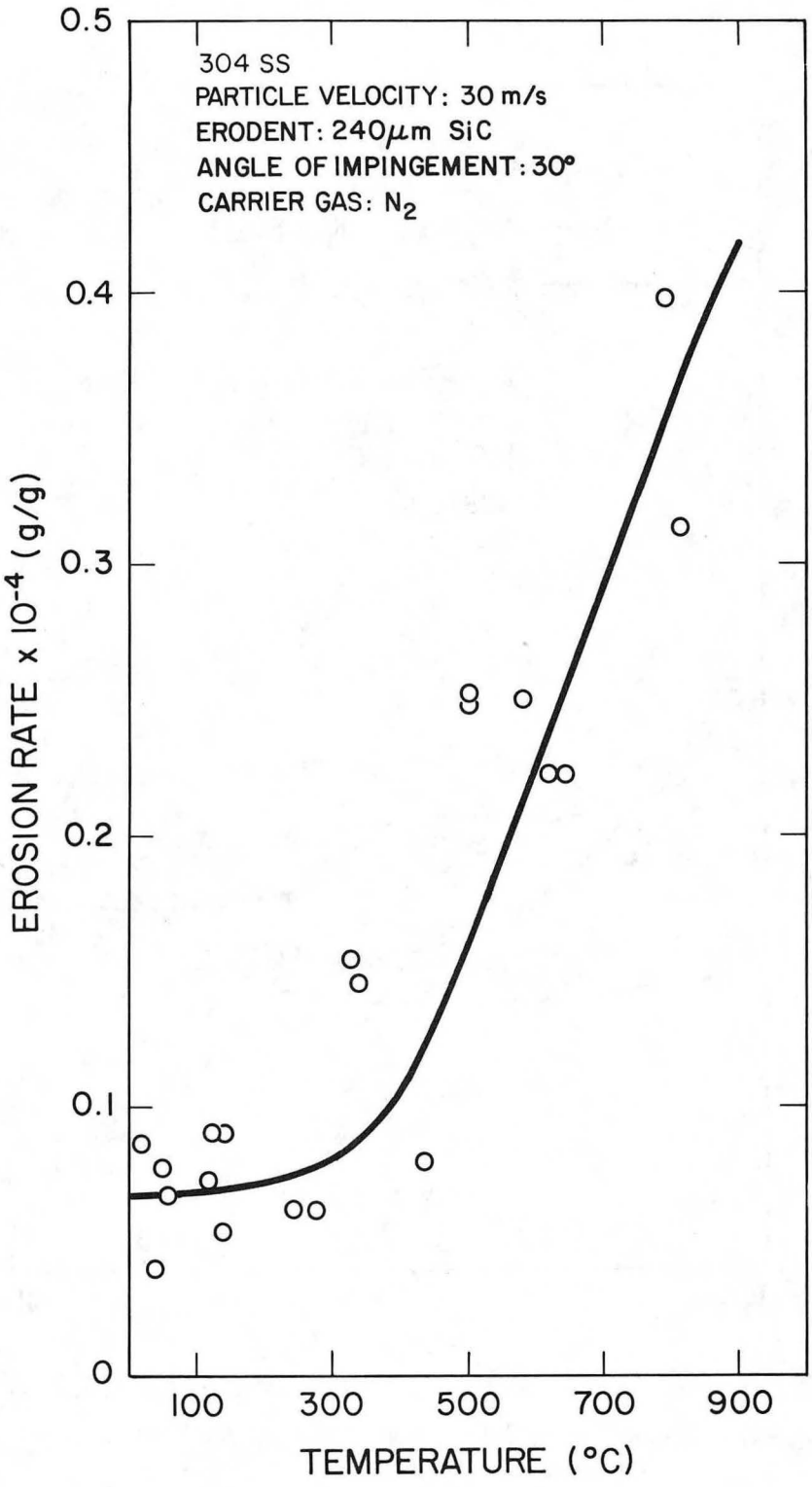

7. Erosion rate v.s. temperature for 304SS.

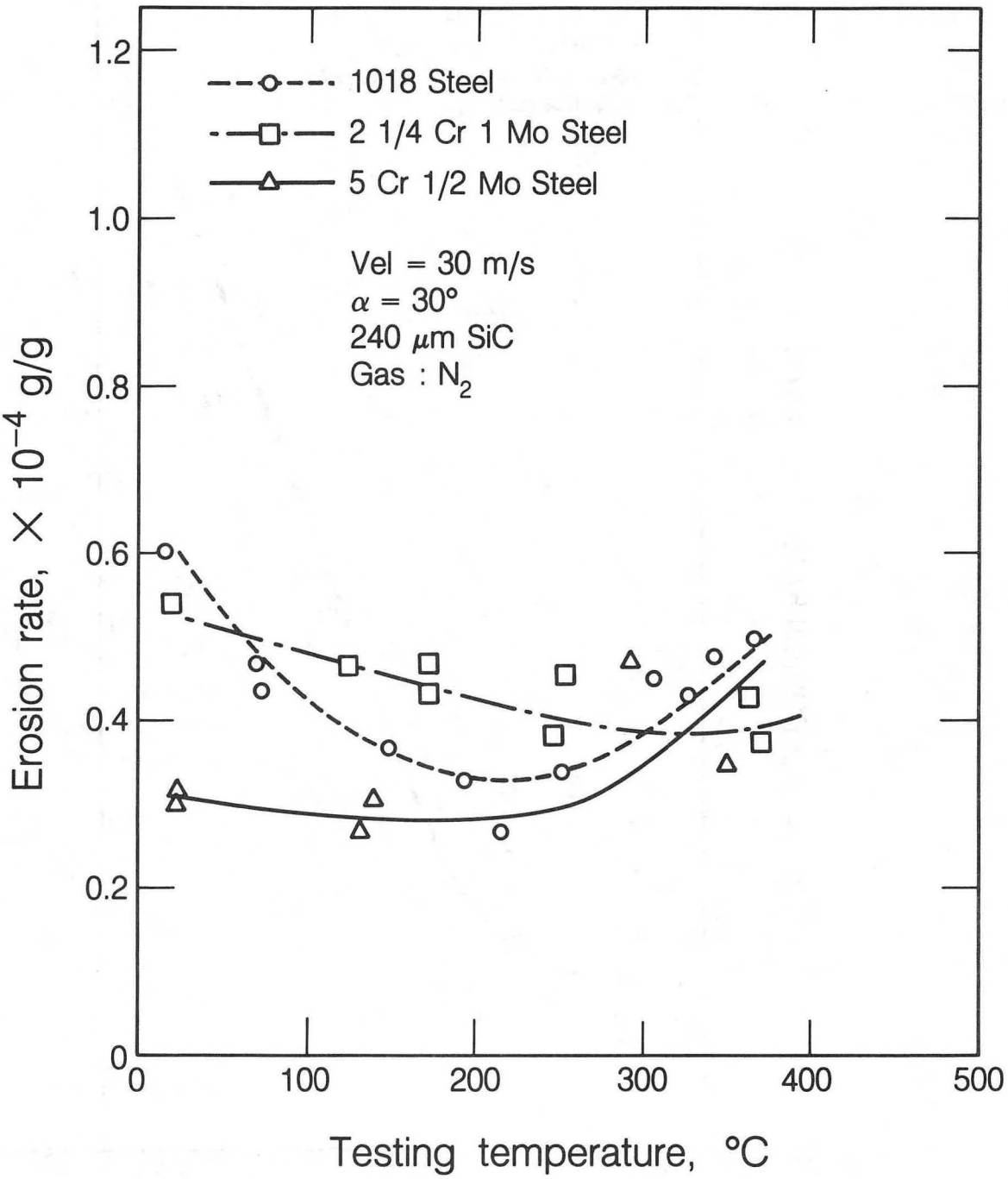

8. Erosion rate v.s. temperature for 1018, 2 1/4Cr1Mo, 5Cr1/2Mo steels.

XBL 848-9886

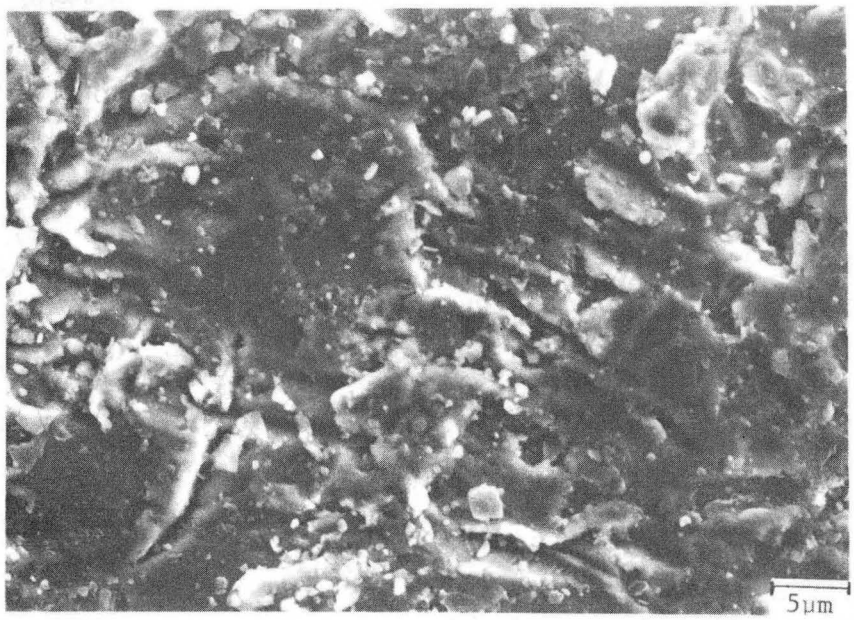

1018 Temp. =370°C

300g of 240μm SiC Vel. =30m/s

Nitrogen gas α =30°

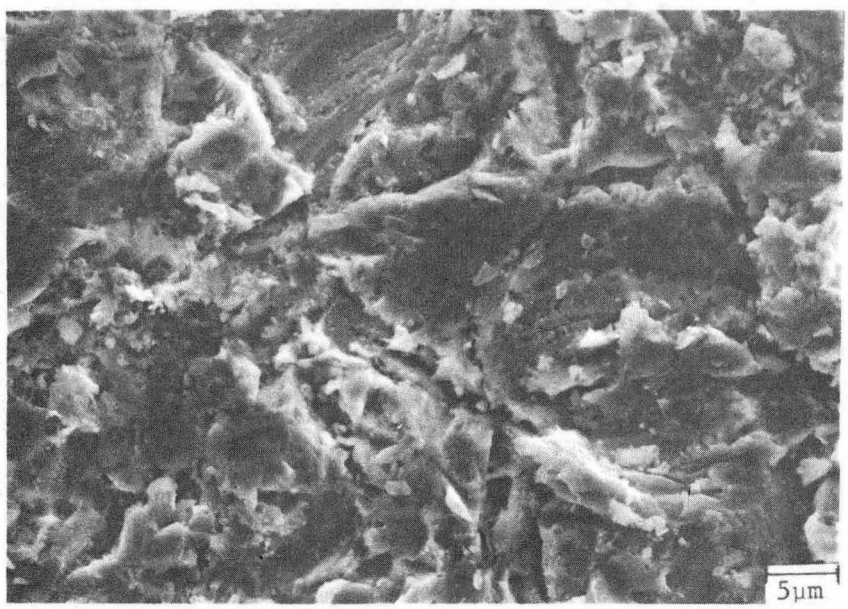

Temp. =20°C

XBB 848-6215

9. Evidence of narrow gouges forming on eroded surface in elevated temperature testing.

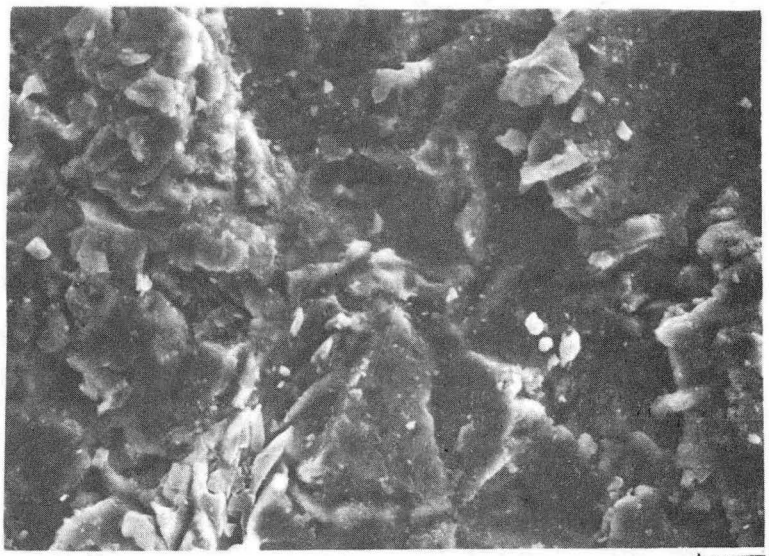

2 1/4 Cr 1 Mo Steel

300g of 240μm SiC
Nitrogen gas

Temp.=370°C
Vel. =30m/s
α =30°

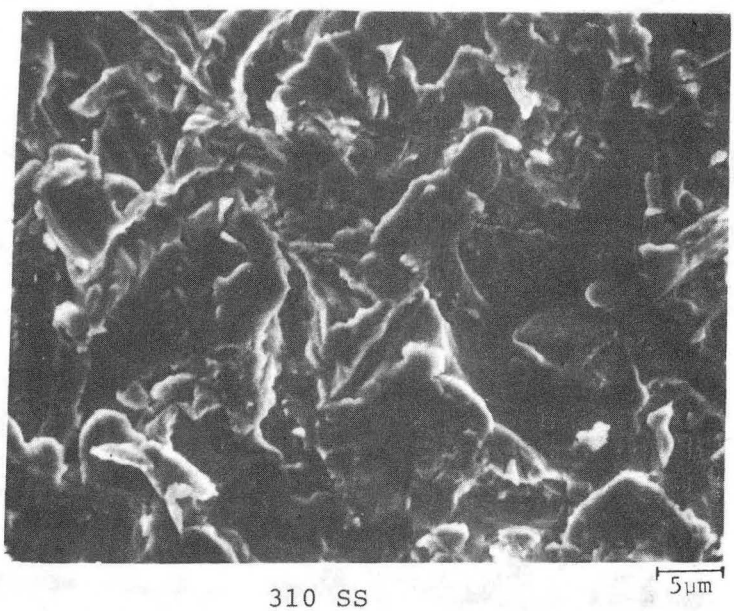

310 SS

300g of 240μm SiC
Nitrogen gas

Temp.=397°C
Vel. =30m/s
α =30°

XBB 837-6074

10. Eroded surfaces of 310SS and 2 1/4Cr1Mo steel.

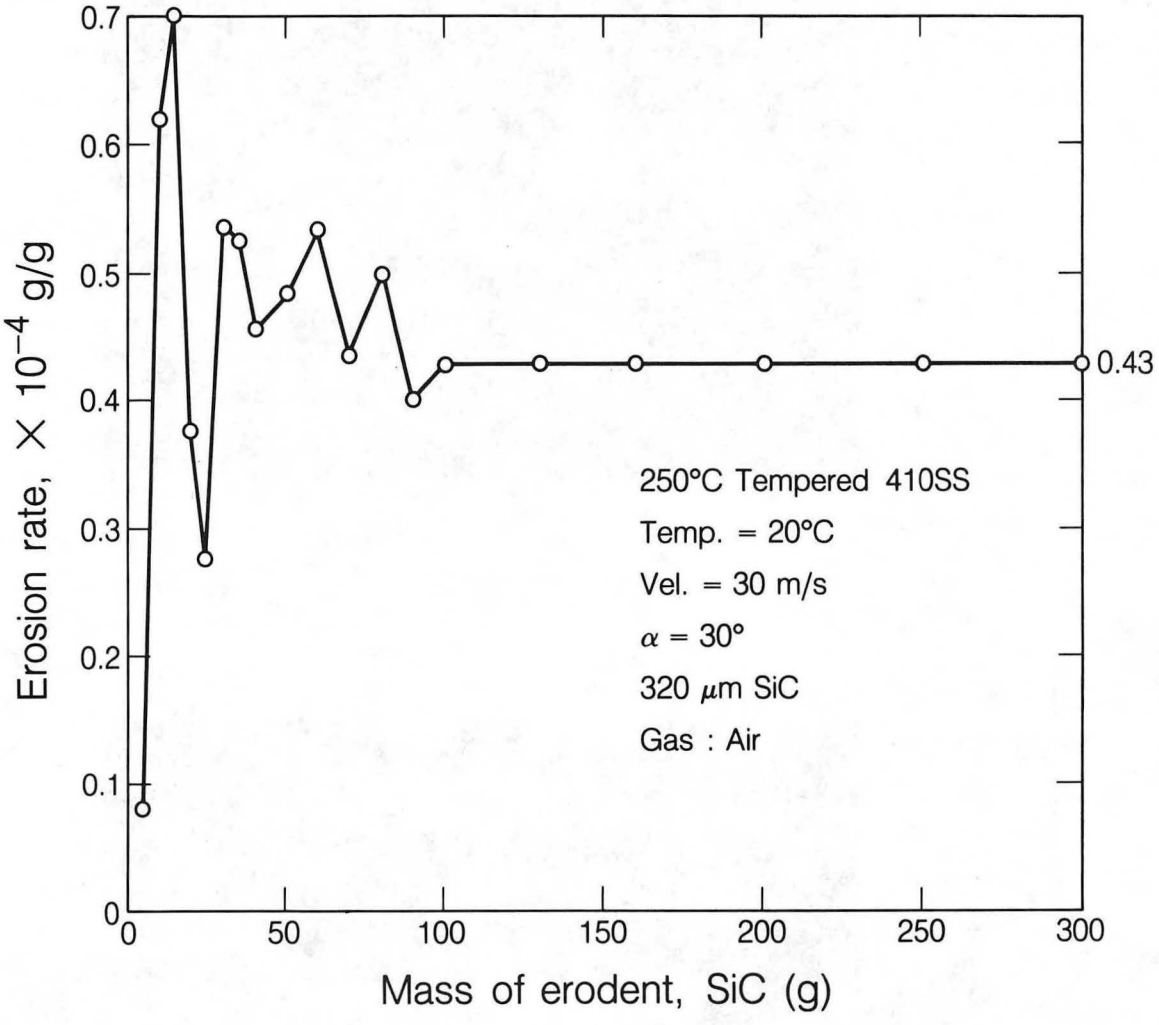

11. Incremental erosion rate curve for 250°C temper 410SS.

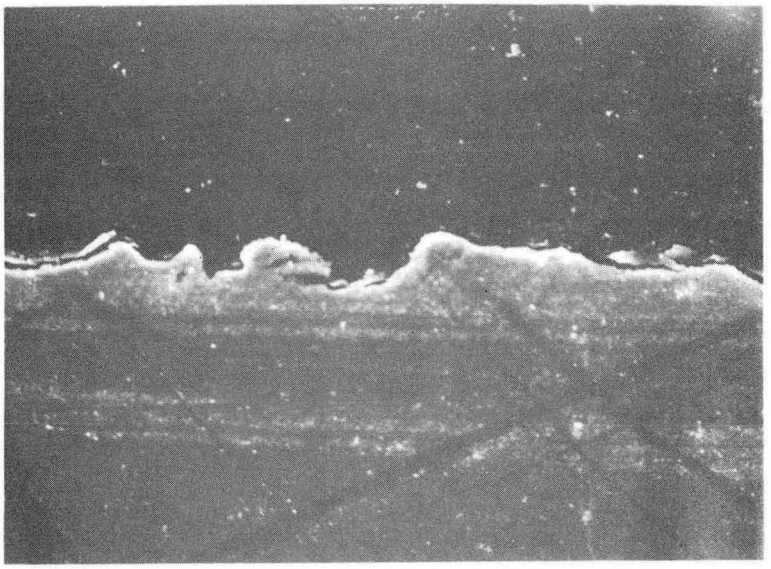

10μm

250°C Tempered 410SS

Temp.=25°C 320μm SiC
Vel. =30m/s Gas : Air
α =30°

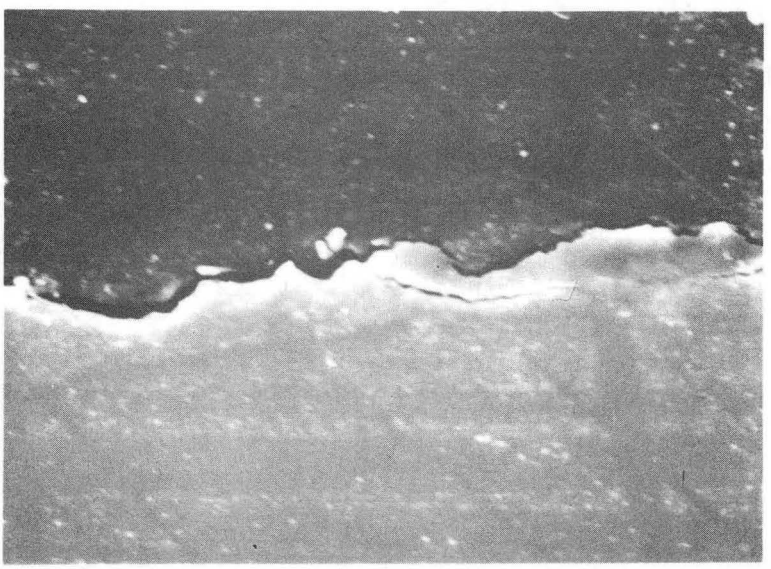

10μm

XBB 848-6216

12. Micrograph of eroded cross section of 250°C temper 410SS eroded at 20°C.

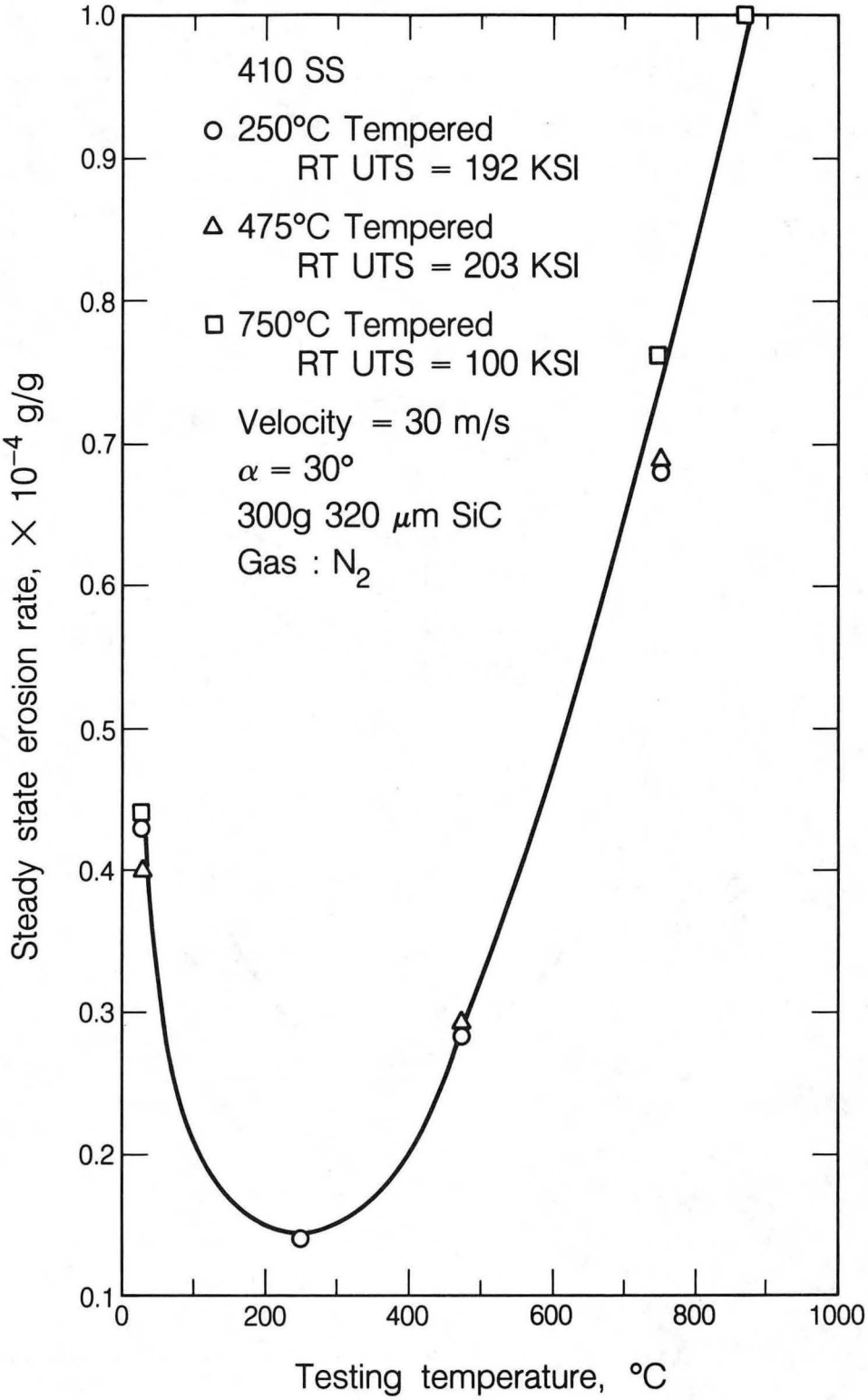

XBL 848-9889

13. Erosion rate v.s. test temperature for 410SS.

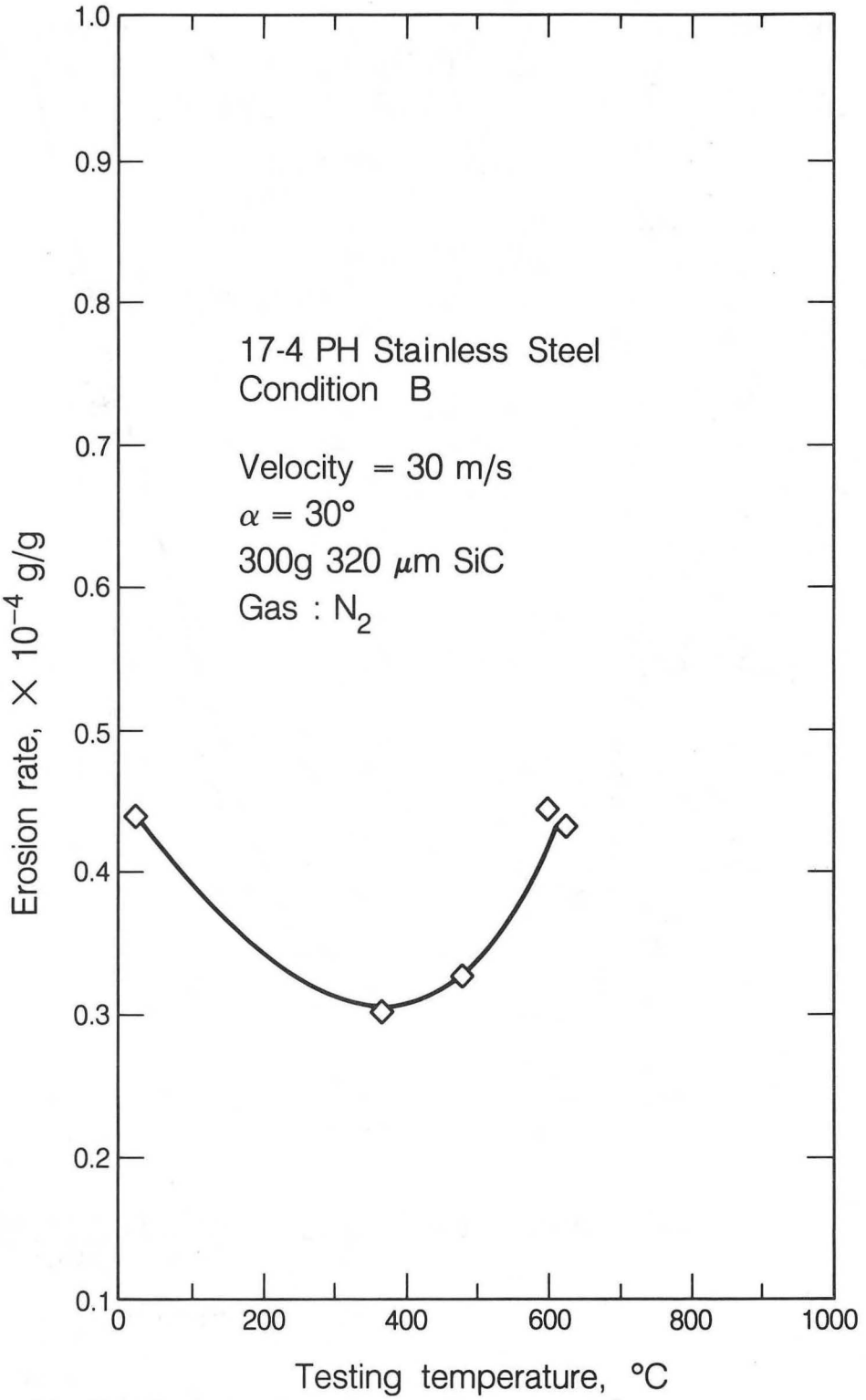

14. Erosion rate v.s. test temperature for 17-PH stainless steel.

XBL 848-9888

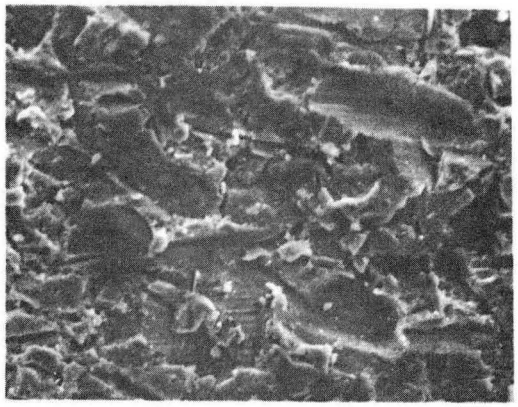

Temp.=600°C
Gas : N_2

10μm

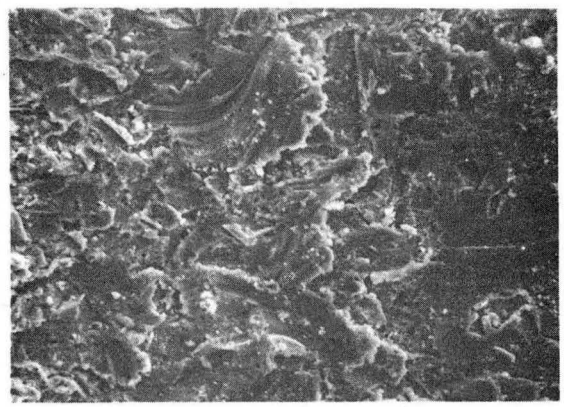

17-4 P H
Vel. =30m/s
α =30°
320μm SiC

Temp.=370°C
Gas : N_2

10μm

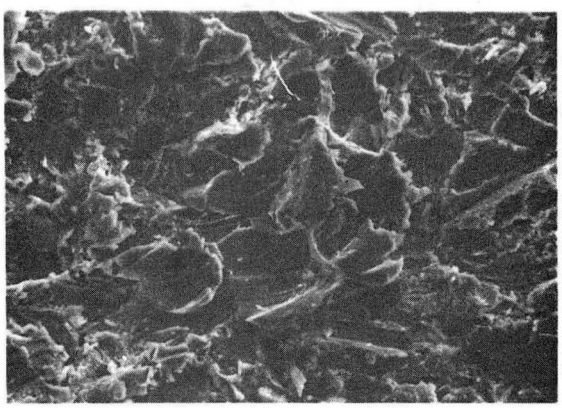

Temp.=25°C
Gas : Air

10μm

XBB 848-6217

15. Surface of eroded 17-4PH at three test temperatures.

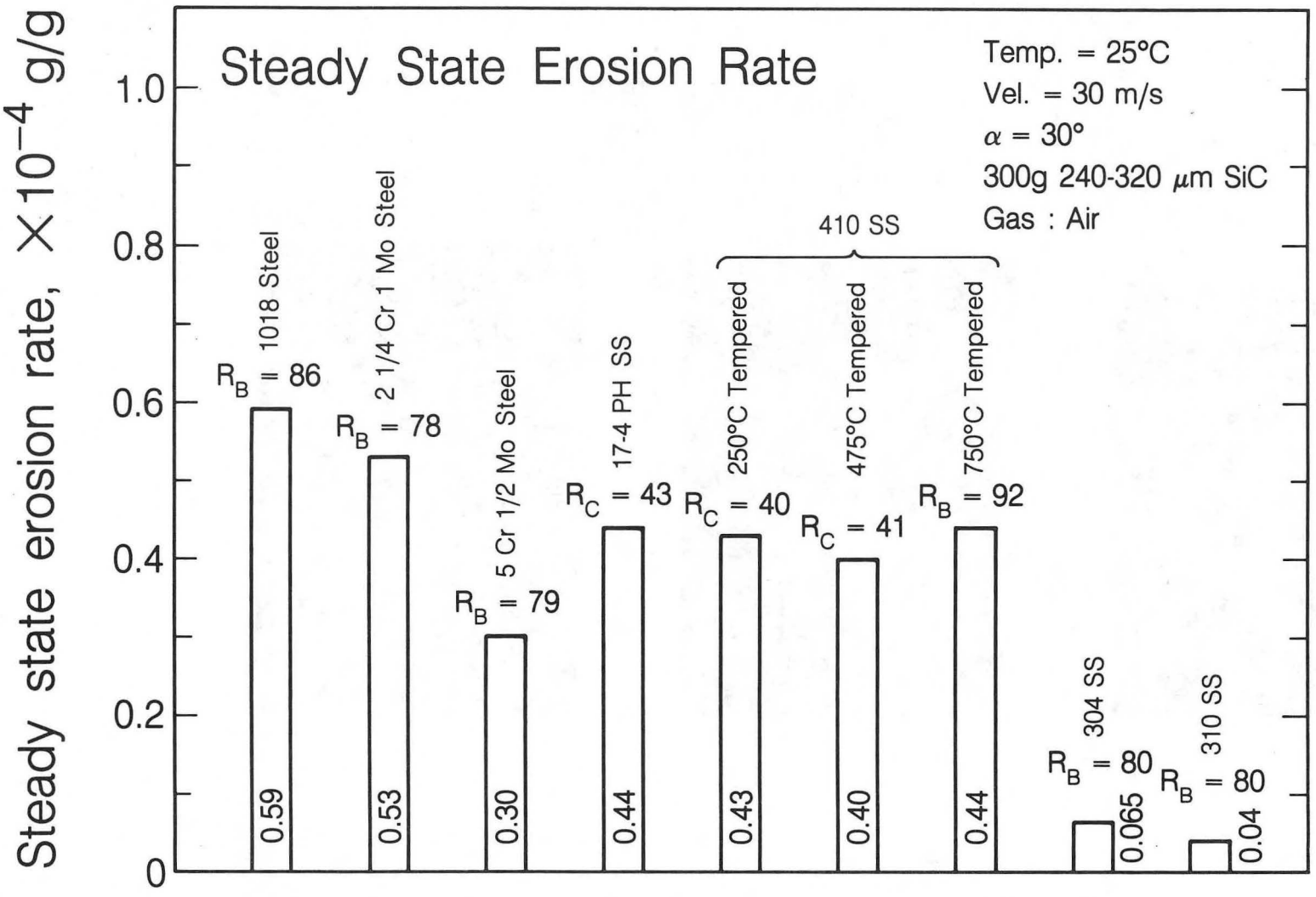

XBL 848-9891

16. Erosion rate bar graph for all alloys at 25°C.

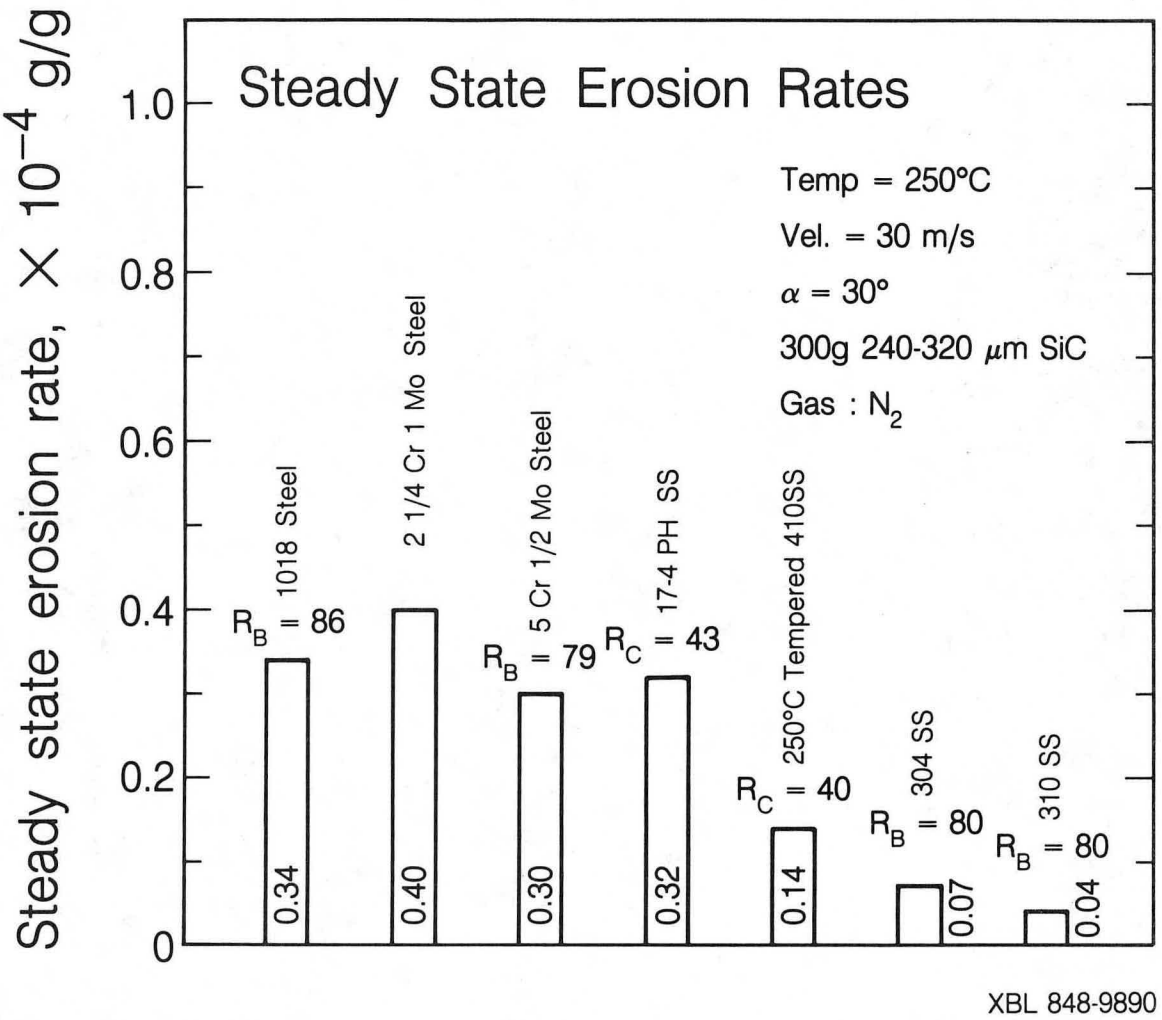

17. Erosion rate bar graph for all alloys tested at 250°C.

DISTRIBUTION LIST

Wate Bakker
EPRI
3214 Hillview Avenue
P.O. Box 10412
Palo Alto, CA 94304

B.R. Banerjee
Ingersoll-Rand Company
P.O. Box 301
Princeton, NJ 08540

K.L. Baumert
Air Products & Chemicals, Inc.
P.O. Box 538
Allentown, PA 18105

S.M. Benford
NASA Lewis Research Center
21000 Brookpark Road
Cleveland, OH 41135

A.E. Biggs
Arco Chemicals
3801 W. Chester Pike
Newtown Square, PA 19073

R. Blickensderfer
Bureau of Mines
P.O. Box 70
Albany, OR 97321

R.A. Bradley, Manager
Fossil Energy Materials Program
Oak Ridge National Laboratory
P.O. Box X
Oak Ridge, TN 37830

Richard Brown
Materials Laboratory
Department of Chemical Engineering
University of Rhode Island
Kingston, RI 02881

DISTRIBUTION LIST cont'd

D.H. Buckley
NASA Lewis Research Center
21000 Brookpark Road
Cleveland, OH 41135

P.T. Carlson, Task Leader
Fossil Energy Materials Program
Oak Ridge National Laboratory
P.O. Box X
Oak Ridge, TN 37830

J. Carpenter
ECUT Program
Oak Ridge National Laboratory
P.O. Box X
Oak Ridge, TN 37830

J.P. Carr
Department of Energy, Office of Fossil Energy
FE-42 Mailstop 3222-GTN
Washington, DC 40525

Hans Conrad
Materials Engineering Department
North Carolina State University
Raleigh, NC 27659

P. Crook
Cabot Corporation
Technology Department
1020 W. Park Avenue
Kokomo, IN 46901

S.J. Dapkunas
Department of Energy, Office of Fossil Energy
Technical Coordination Staff FE-14
Mailstop C-156 GTN
Washington, DC 40525

DOE Technical Information Center
P.O. Box 62
Oak Ridge, TN 37830

W.A. Ellingson
Argonne National Laboratory
9700 South Cass Avenue
Argonne, IL 60439

DISTRIBUTION LIST cont'd

J. Gonzales
GTE
Chemical & Metallurgical Division
Hawes Street
Towanda, PA 18848

A. Hammarsten
Teknikum
P.O. Box 534, S-751 21
Uppsala
SWEDEN

E. Haycock
Westhollow Research Center
Shell Development Company
P.O. Box 1380
Houston, TX 77001

J.M. Hobday
Department of Energy
Morgantown Energy Technology Center
P.O. Box 880
Morgantown, WV 26505

E.E. Hoffman, Manager
National Materials Program
Department of Energy
Oak Ridge Operations
P.O. Box E
Oak Ridge, TN 37830

J.A.C. Humphrey
Mechanical Engineering Department
University of California
Berkeley, CA 94720

I.M. Hutchings
University of Cambridge
Department of Metallurgy
Pembroke Street
Cambridge
ENGLAND

Sven Jansson
Stal-Laval Turbin AB
Finspong S-61220
SWEDEN

DISTRIBUTION LIST cont'd

R.R. Judkins
Fossil Energy Materials Program
Oak Ridge National Laboratory
P.O. Box X
Oak Ridge, TN 37830

James Keiser
Oak Ridge National Laboratory
P.O. Box X
Oak Ridge, TN 37830

M.K. Keshavan
Union Carbide Corporation
Coating Services Department
1500 Polco Street
Indianapolis, IN 46224

T. Kosel
University of Notre Dame
Dept. of Metallurgical Engineering
& Materials Science
Box E
Notre Dame, IN 46556

L. Lanier
FMC-Central Engineering Laboratory
1185 Coleman Avenue
Santa Clara, CA 95052

N.H. MacMillan
Pennsylvania State University
167 Materials Research Laboratory
University Park, PA 16802

P.K. Mehrotra
Kennemetal Inc.
1011 Old Salem Road
Greensburg, PA 15601

Ken Magee
Bingham-Williamette Co.
2800 N.W. Front Avenue
Portland, OR 97219

T. Mitchell
Case Western Reserve University
Department of Metallurgy
Cleveland, OH 44106

DISTRIBUTION LIST cont'd

Fred Pettit
Dept. of Metallurgy & Materials Engineering
University of Pittsburgh
Pittsburgh, PA 15261

R.A. Rapp
Metallurgical Engineering
116 W. 19th Avenue
The Ohio State University
Columbus, OH 43210

D.A. Rigney
Metallurgical Engineering
116 W. 19th Avenue
The Ohio State University
Columbus,OH 43210

A.W. Ruff
Metallurgy Division
National Bureau of Standards
B-266 Materials
Washington, DC 20234

Alberto Sagues
IMMR - University of Kentucky
763 Anderson Hall
Lexington, KY 40506

Gordon Sargent
University of Notre Dame
Dept. of Metallurgical Engineering & Materials Science
Box E
Notre Dame, IN 46556

Paul Shewmon
Dept. of Metallurgical Engineering
116 W. 19th Avenue
Columbus, OH 43210

Gerry Sorell
EXXON Research & Engineering Company
P.O. Box 101
Florham Park, NJ 07932

Carl A. Stearns
Head, High Temperature Chemistry Section
NASA, Lewis Research Center 106-1
21000 Brookpark Road
Cleveland, OH 44135

DISTRIBUTION LIST cont'd

John Stringer
University of California
Lawrence Berkeley Laboratory
Mailstop 62/203
Berkeley, CA 94720

Widen Tabakoff
Dept. of Aerospace Engineering
University of Cincinnati
Cincinnati, OH 45221

Edward Vesely
IITRI
10 West 35th Street
Chicago, IL 60616

J.J. Wert
Metallurgy Department
Vanderbilt University
P.O. Box 1621, Sta. B
Nashville, TN 37235

J.C. Williams
Dept. of Metallurgy & Materials Science
Carnegie-Mellon University
Schenley Park
Pittsburgh, PA 15213

S. Wolf
Department of Energy
Basic Energy Sciences Office
Division of Materials Sciences
Washington, DC 20545

Ian Wright
Materials Science Division
Battelle Memorial Institute
505 King Avenue
Columbus, OH 43201

C.S. Yust
Metals and Ceramics Division
Oak Ridge National Laboratory
P.O. Box X
Oak Ridge, TN 37830

This report was done with support from the Department of Energy. Any conclusions or opinions expressed in this report represent solely those of the author(s) and not necessarily those of The Regents of the University of California, the Lawrence Berkeley Laboratory or the Department of Energy.

Reference to a company or product name does not imply approval or recommendation of the product by the University of California or the U.S. Department of Energy to the exclusion of others that may be suitable.

TECHNICAL INFORMATION DEPARTMENT
LAWRENCE BERKELEY LABORATORY
UNIVERSITY OF CALIFORNIA
BERKELEY, CALIFORNIA 94720